Fusion Engineering and Design 117 (2017) 150–156

Contents lists available at ScienceDirect

Fusion Engineering and Design

journal homepage: www.elsevier.com/locate/fusengdes

Effect of progressively increasing lithium conditioning on edge transport and stability in high triangularity NSTX H-modes

R. Maingi[a,*], J.M. Canik[b], R.E. Bell[a], D.P. Boyle[c], A. Diallo[a], R. Kaita[a], S.M. Kaye[a], B.P. LeBlanc[a], S.A. Sabbagh[d], F. Scotti[e], V.A. Soukhanovskii[e], and the NSTX team

[a] Princeton Plasma Physics Laboratory, 100 Stellarator Road, Princeton, NJ 08543, USA
[b] Oak Ridge National Laboratory, Oak Ridge, TN, USA
[c] Princeton University, Princeton, NJ, USA
[d] Columbia University, New York, NY, USA
[e] Lawrence Livermore National Laboratory, Livermore, CA, USA

ARTICLE INFO

Article history:
Received 8 January 2016
Received in revised form 24 June 2016
Accepted 28 June 2016
Available online 19 July 2016

PACS:
52.40.Hf
52.25.-b
52.30.-q
52.55.-s

Keywords:
NSTX
Lithium
Recyling
Pedestal
Energy confinement

ABSTRACT

A sequence of H-mode discharges with increasing levels of pre-discharge lithium evaporation ('dose') was conducted in high triangularity and elongation boundary shape in NSTX. Energy confinement increased, and recycling decreased with increasing lithium dose, similar to a previous lithium dose scan in medium triangularity and elongation plasmas. Data-constrained SOLPS interpretive modeling quantified the edge transport change: the electron particle diffusivity decreased by 10–30x. The electron thermal diffusivity decreased by 4x just inside the top of the pedestal, but increased by up to 5x very near the separatrix. These results provide a baseline expectation for lithium benefits in NSTX-U, which is optimized for a boundary shape similar to the one in this experiment.

1. Introduction and background

Lithium has been applied to plasma-facing components (PFCs) in fusion devices to improve performance with a number of delivery techniques. In addition to evaporation of metallic lithium discussed below, lithium pellets were injected in TFTR [1], DIII-D [2], and NSTX [3], with modest to moderate short-term performance enhancement. Lithium was also via a laser-based aerosol delivery system, which improved the nτT triple product by more than a factor of 50 in TFTR [4]. In addition, lithium powder was delivered as an aerosol [5] to improve performance in DIII-D [6] and EAST [7]. Also, lithium granules were injected into EAST [8] and DIII-D [9], to ameliorate ELM size by increasing the natural ELM frequency. Finally liquid lithium was used in a static liquid lithium divertor configuration in NSTX [10], a liquid lithium limiter in FTU [11], as a liquid on heated walls in LTX [12,13], and as a flowing liquid lithium limiter in HT-7 [14] and EAST [15]. A recent review provides additional details [16].

Lithium was evaporated via ovens into TJ-II [17] and NSTX [18–20]. In NSTX, recycling was reduced and confinement was improved; also ELMs were eliminated [21,22], owing to an inward shift of the electron density profile relative to the electron temperature profile very close to the separatrix, which stabilized peeling-ballooning modes [23,24]. The magnitude of the increase in energy confinement in NSTX increased with the pre-discharge lithium evaporation 'dose' [25,26]. In addition the density and pressure profile steep gradient regions shifted progressively away from the separatrix with increasing does. Interpretive simulations with the SOLPS code indicated that the recycling coefficient at the divertor target dropped with increasing lithium evaporation, from ~R = 0.99 to ~R = 0.85–0.90 during this scan, and the core fueling rate dropped by 40–60% [27,28]. The required cross-field electron particle diffusivity D_e and electron thermal diffusivity χ_e increased modestly in the last 5% of normalized poloidal flux ψ_N

* Corresponding Author at: PPPL, 100 Stellarator Road, Princeton, NJ 08543, USA.
E-mail address: rmaingi@pppl.gov (R. Maingi).

http://dx.doi.org/10.1016/j.fusengdes.2016.06.058
0920-3796/

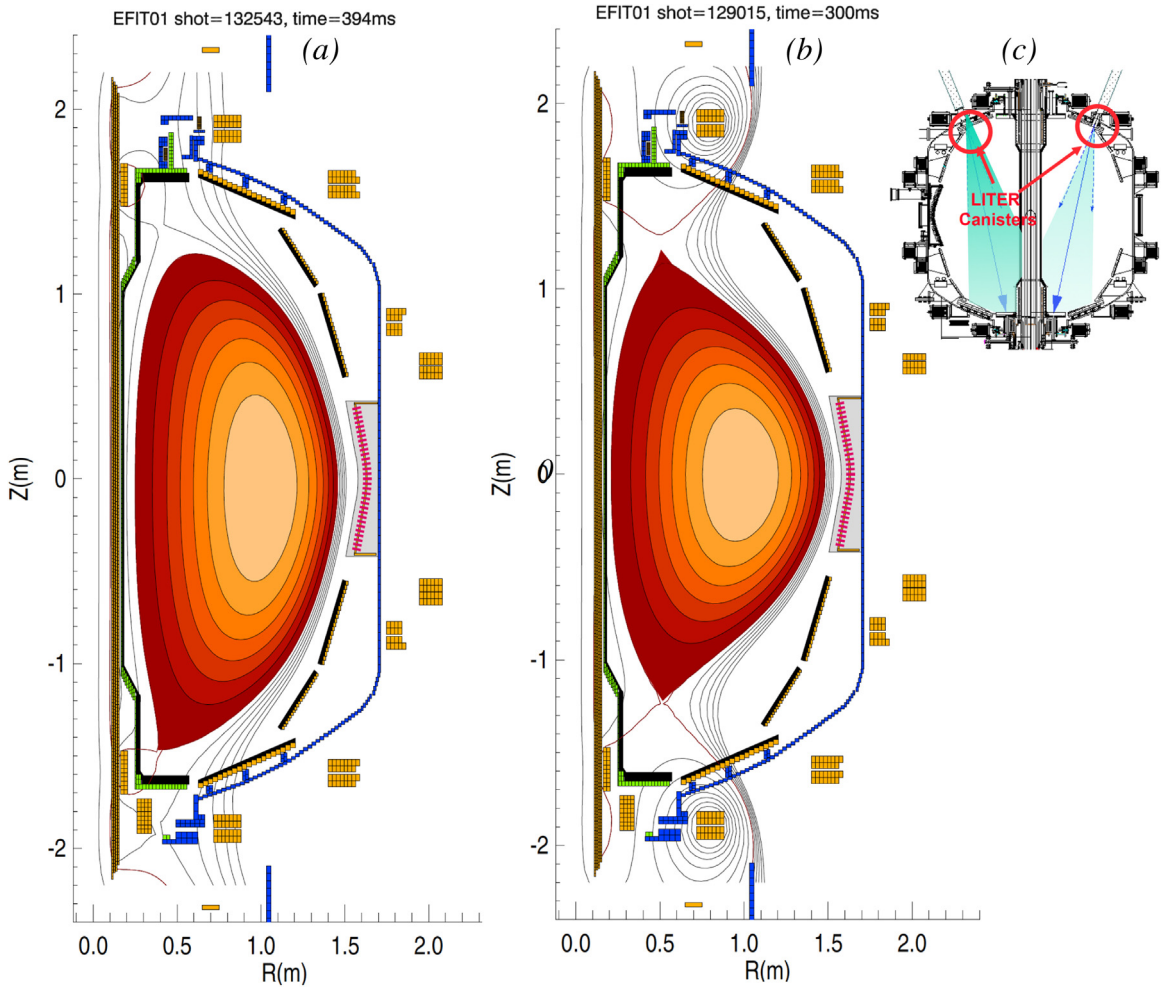

Fig. 1. Comparison of high and low δ shapes (a) and (b) with centroid of lithium evaporator deposition (c).

near the separatrix, but decreased inside of that region, consistent with the observed steeper gradients and improved confinement [29].

The NSTX experiments and analysis mentioned in the last paragraph were performed in a moderate triangulariy $\delta \sim 0.45$, elongation $\kappa \sim 1.8$ boundary shape, and then repeated in a high triangularity $\delta \sim 0.65$, elongation $\kappa \sim 2.2$ boundary shape, with similar global trends regarding discharge modifications as a function of lithium evaporation [30]. A comparison of these boundary plasma shapes is shown in Fig. 1, along with a schematic of two toroidally separated overhead LIThium EvapoRators ("LITER") in NSTX. Note in particular that the centroid of LITER deposition was very close to the outer divertor strike point in the highly shaped plasma, whereas it was in the private flux region in the weakly shaped plasma. Here we present additional details of the progression of the lithium dose scan in the highly shaped discharge prototypical of NSTX-U, along with new SOLPS interpretive modeling to quantify the change in divertor recycling coefficient and cross-field transport rates.

2. Trends as a function of pre-discharge lithium

This was the first experiment in this particular campaign in which lithium was used; previous discharges used periodic boronization and inter-shot helium glow discharge cleaning. The pre-discharge lithium dose, along with the integral deposition, is shown as a function of shot number in Fig. 2. After obtaining ~10 reference discharges with both 5 and 6 MW neutral-beam injected (NBI) power, lithium was introduced for seven discharges at a dose ~150 mg. The next eight discharges used ~250 mg per discharge. The next six discharges varied the lithium dose between 250 and 500 mg each, with some alternation of high and low doses

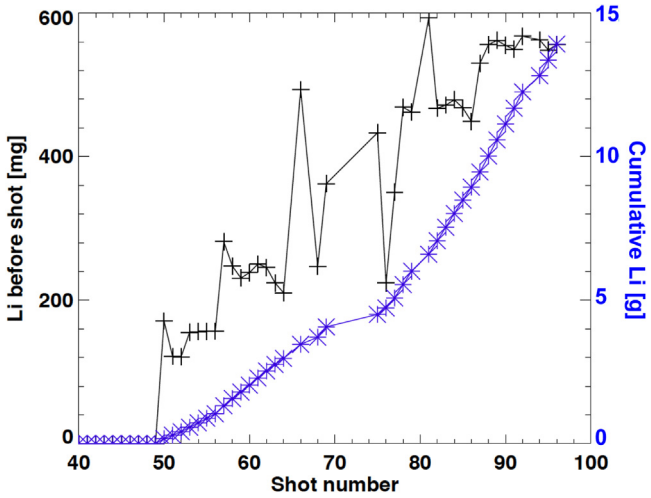

Fig. 2. Lithium deposition before each discharge (black plus symbols) and cumulative (blue stars). The actual discharge number is obtained by adding 132500 to the x-axis (for interpretation of the references to colour in this figure legend, the reader is referred to the web version of this article).

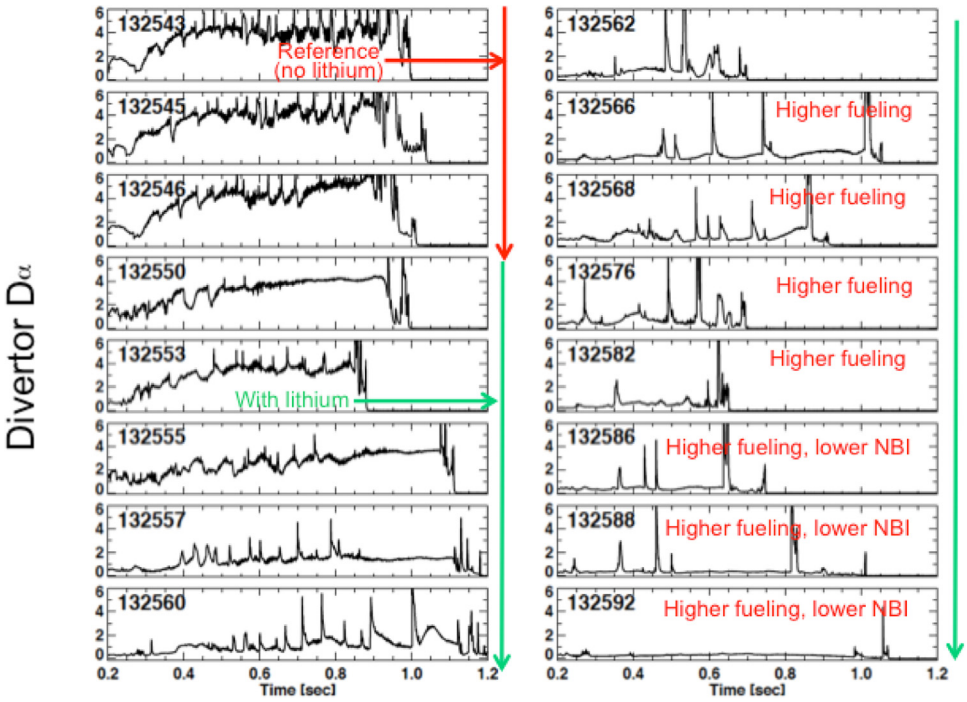

Fig. 3. Evolution of divertor Dα from selected discharges from the lithium evaporation scan. Gas fueling was held constant until #132566, and heating power was reduced starting with #132586.

to assess hysteresis. The following eight discharges used ~450 mg per discharge, while the final nine discharges used ~500–550 mg per discharge. The effects observed in this experiment depended mostly on the lithium dose between discharges, with a minor effect related to the integral dose.

Fig. 3 shows the divertor Dα emission vs. time for select discharges during the lithium dose scan. The reference discharges were fairly well optimized in terms of pulse length (up to ~1 s) and discharge stored energy. Lithium was introduced before #132550, with doses as indicated in Fig. 2. It can be seen that the baseline Dα was progressively reduced with increasing lithium dose. The external gas fueling was held constant until discharge #132566, and the NBI power was reduced to 4 MW for #132586. Generally the pulse lengths were longer with lithium conditioning once the fueling and NBI power was optimized. The longest pulses achieved were up to 1.2 s, e.g. #132557–132560.

Certain details of this lithium dose scan, e.g. the trends of Dα emission from the upper and lower divertors, as well as normalized energy confinement and midplane neutral pressure as a function of lithium dose for this high triangularity shape were presented previously [30]. This paper builds on that previous work, with in-depth edge transport modeling and recycling analysis; hence, a few details from the previous paper are summarized here for additional insights into the trends. Generally the Dα emission and neutral pressure decreased with increasing lithium dose, while normalized energy confinement increased. The trends with lithium dose in this high triangularity shape were similar to those observed during a Li dose scan with weaker shaping [24,25], except that the rapid drop in lower divertor baseline Dα emission, which signifies the transition from high recycling to sheath limited divertor heat transport, occurred at a dose ~200 mg in the high triangularity dose scan, as compared to ~500 mg in the dose scan for the weakly shaped discharges. In addition the lower divertor baseline Dα emission dropped by 90% at the highest lithium dose in this lithium dose scan at high shaping, as compared to a ~70% drop observed during the scan at low shaping. Both of these differences are qualitatively consistent with the centroid of lithium deposition being closer to the outer strike point at high shaping than low shaping [30]. Finally the trends in this experiment also agree semi-quantitatively with independent analysis of other discharges with 190 mg and 600 mg lithium dose in this discharge shape [31], i.e. discharges that were not part of this systematic scan.

A comparison of the evolution of three discharges during the experiment is presented in Fig. 4. These three discharges were used in the interpretive SOLPS modeling to quantify the reduction in divertor recycling coefficient and edge cross-field transport. Panel (a) displays plasma current I_p, panel (b) the NBI power P_{NBI}, panel (c) the line-averaged electron density from Thomson Scattering, panel (d) the normalized pressure β_N, panel (e) the energy confinement time normalized to the ITER H97 L-mode scaling law [32], panel (f) the radiated power in the core, and panel (g) the lower divertor Dα emission. The normalized pressure is defined by $\beta N = \beta t B_t a_m / I_p$, where β_t is the average plasma pressure normalized to the on-axis vacuum toroidal field: $\beta\tau = 4\mu_0 W_{MHD}/(3 V_p B_t^2)$. Also B_t is the toroidal field, a_m the minor radius, W_{MHD} the stored energy from equilibrium reconstructions, V_p the plasma volume, and μ_0 the permittivity of free space. The P_{NBI} was reduced from 6 –> 5 –> 4 MW with increasing lithium dose to keep the plasma below the global stability limit $\beta N \leq 6$ (panels (b), (e)). The normalized confinement improved with increassing lithium dose (panel (e)). Note that the radiated power (panel (f)) was slowly increasing in the discharges with lithium conditioning; this is a commonly observed state when ELMs were eliminated (panel (g)) with lithium evaporation in NSTX [22], thereby eliminating the periodic flushing of impurities. In addition the resulting profile changes neoclassical transport so that carbon and metallic impurities accumulated in the core, causing the temporal increased in radiated power [33].

3. SOLPS modeling

The SOLPS code [34] was used in interpretive analysis mode to quantify the changes in divertor recycling and cross-field transport; the procedure has been described in detail elsewhere for the discharges with moderate boundary shapes [27,29]. In brief, the

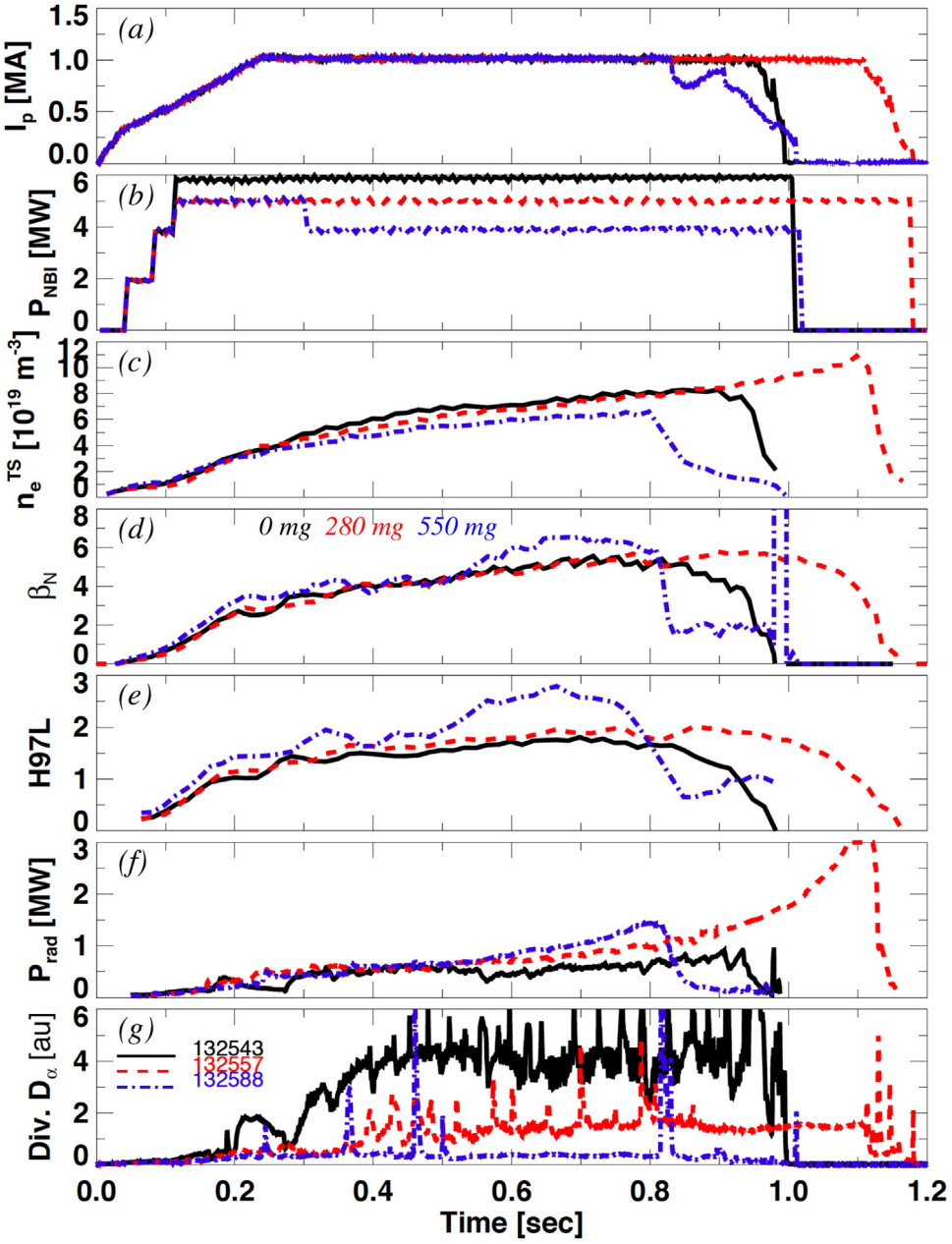

Fig. 4. Comparison of reference discharge (black) with intermediate (red) and high (blue) pre-discharge lithium evaporation. The NBI power was reduced modestly to stay below the global stability limit.

divertor Dα peak emission is the primary constraint on the divertor target recycling coefficient, the divertor peak heat flux is the primary constraint on the separatrix location in the reconstructed equilibrium (via power balance), and the density and temperature profiles serve to set the cross-field transport particle and thermal diffusivities.

A comparison between measured and simulated profiles is given in Fig. 5 for the reference boronized discharge before lithium evaporation. The midplane n_e, T_e, and T_i profiles as a function of normalized poloidal flux ψ_N are obtained by ELM synchronization of multiple time slices to the last 50% of the ELM cycle. Note that $\psi_N = (\psi_0 - \psi(\rho))/(\psi_0 - \psi_{sep})$ with ψ_0 and- ψ_{sep} being the poloidal flux at the magnetic axis and separatrix respectively. A comparison of the divertor profile data and simulations is plotted in physical space along the divertor target, from single time slices.

A few points are highlighted. First the T_i profile in the SOL is below the measured values. This is because the measurements in the SOL are representative of the fast ion population, as opposed to a themal population. As a result, the T_e profile is used as a guideline to set the SOL cross-field ion heat transport. This comment applies to all three simulated timeslices in the succeeding paragraphs. In addition, the divertor Dα measurement saturated at a relatively low level; other measurements suggested the peak instensity was up to $\sim 10^{23}$ photons/m^2/sec. Hence the simulated Dα was substantially higher than the measured value. The simulation used a divertor recycling coefficient $R_p = 0.995$, and a simulation using a value closer to unity would have been a somewhat more accurate representation. In addition the inner divertor Dα peak for $R < 0.3$ m from the simulation is physically on the center stack vertical section (Fig. 1); due to the viewing geometry, that peak is not measured by the 1-D CCD camera [35]. This measurement limitation also applies

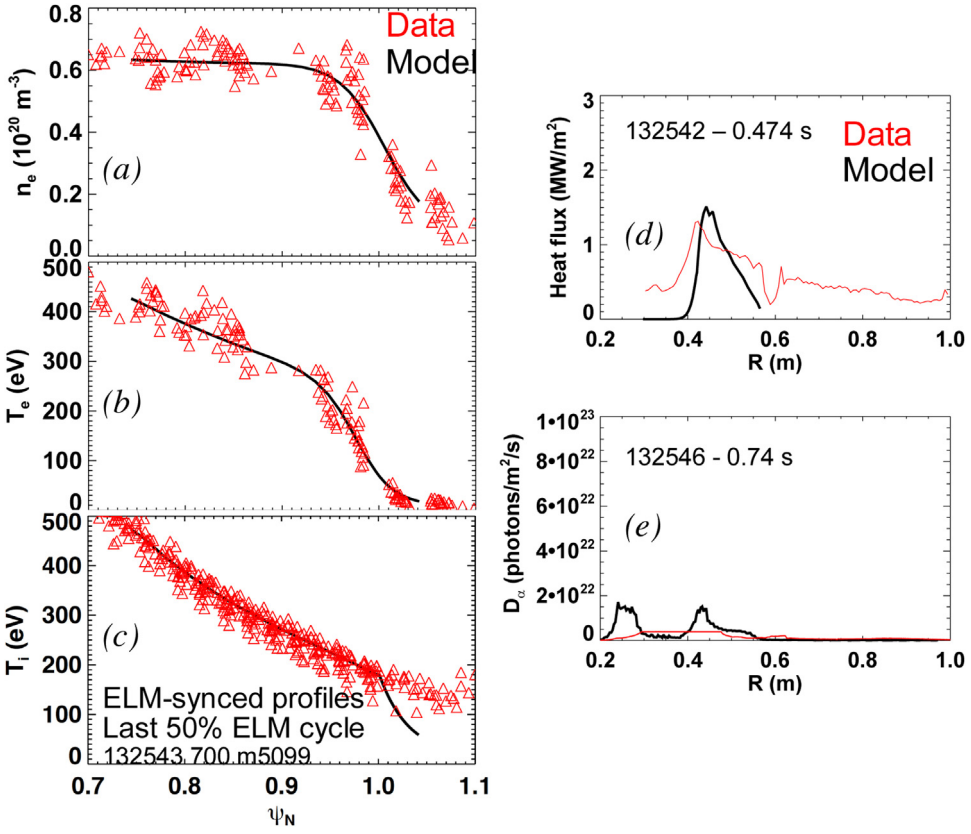

Fig. 5. Composite plasma profiles synced to the last 50% of the ELM cycle from reference boronized discharges with 6 MW NBI power: (a) electron density n_e, (b) electron temperature T_e, and (c) ion temperature T_i, The red symbols are data, and the solid black curve comes from SOLPS modeling. The lower divertor heat flux and peak Dα are shown in panels (d) and (e) respectively. The divertor Dα measurement saturated above 4×10^{21} photons/m^2/s (for interpretation of the references to colour in this figure legend, the reader is referred to the web version of this article).

to the simulations presented in Figs. 6 and 7 also. Nonetheless, the baseline simulation was deemed sufficient as it represented a high recycling (but not "partially detached" [36]) solution.

Fig. 6 compares the measured profiles with simulations for the discharges with ~280 mg lithium dose. As can be seen by the plots, the simulated profiles and measured profiles are in good agreement except for the divertor Dα value, which is again underestimated. The divertor recycling coefficient $R_p = 0.94$, and probably should have been increased for a better match with data, but for the purpose of this study, the agreement was deemed acceptable.

Finally the measured and simulated profiles for the discharges with ~550 mg lithium dose are shown in Fig. 7. Overall the simulations and measured profiles are in very good agreement. These simulations used divertor recycling coefficient $R_p = 0.90$. Note that this divertor recycling coefficient is moderately higher than the $R_p = 0.8$–0.85 inferred from UEDGE analysis of the individual 600 mg discharge mentioned previously [31].

In addition to quantifying the change in divertor recycling coefficient, the other primary purpose of the SOLPS simulations is to quantify the change in electron transport in the edge region near the separatrix. The simulations can only provide effective transport coefficients, i.e. separate diffusion and pinch terms cannot be accurately determined because this type of interpretive analysis is time independent.

Fig. 8 shows the radial D_e and χ_e obtained from the SOLPS simulations to reproduce the measured profiles. The D_e decreased monotonically inside the separatrix, by factors of 10–30x, when comparing the reference and highest lithium dose discharge. On the other hand, the χ_e increased by up to 10x in the last 1–1.5 cm nearest the separatrix, but decreased by 5x inside of that region. The near-separatrix region increase in thermal transport can be understood conceptually because a higher diffusivity is needed to drive the same cross-field heat flux at the reduced edge density obtained with lithium conditioning, e.g. see the profile changes shown elsewhere [30]. The reduction in χ_e inside of that region was also observed with SOLPS analysis from the moderately shaped discharges; microstability analysis indicated a reduction in the drive for microtearing modes [37]. Quantitatively the reduction in D_e and χ_e in these highly shaped discharges is very similar to those observed at moderate shaping [25,29].

4. Summary and conclusions

In this paper we have used SOLPS modeling to quantify the reduction in divertor recycling and change in edge transport for low and high lithium dose, as compared to a reference boronized discharge without lithium, for a strongly shaped boundary NSTX H-mode discharge. The divertor recycling coefficient dropped from between 0.99 and 1.0, to ~0.9 for a 550 mg lithium dose. In addition, both the particle and electron thermal diffusivity dropped substantially in a broad region 1–4 cm radially inward of the separatrix, although electron transport within 1 cm of the separatirx increased substantially. Overall the results were very similar to a comparable lithium dose scan conducted in moderately shaped discharges.

Overall these results bode well for lithium usage to enhance plasma performance and reduce recycling in NSTX-U [38], which is designed to use a highly shaped boundary plasma as in this study. Note that the lithium evaporators in NSTX-U will have the same geometry as in NSTX; thus, the centroid of the deposition will differ slightly from these experiments, owing to the larger center

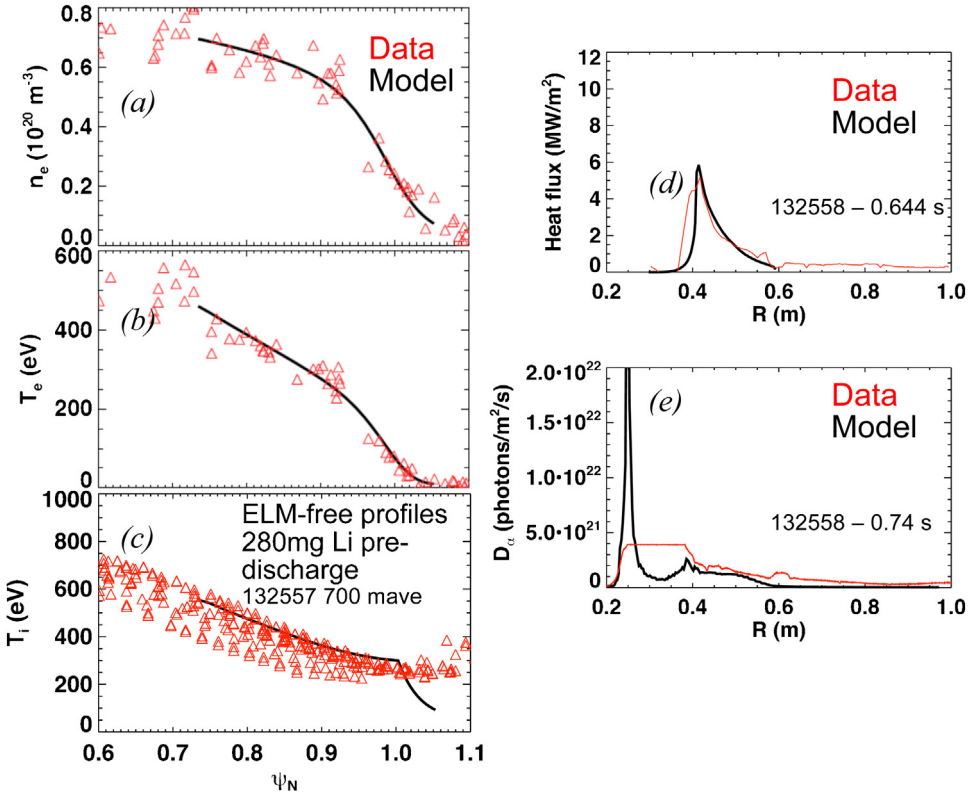

Fig. 6. Composite plasma during ELM-free phases from discharges with 5 MW NBI power and ~280 mg lithium dose: (a) n_e, (b) T_e and (c) T_i. The red symbols are data, and the solid black curve comes from SOLPS modeling. The lower divertor heat flux and peak Dα are shown in panels (d) and (e) respectively. The divertor Dα measurement saturated above 4×10^{21} photons/m2/s (for interpretation of the references to colour in this figure legend, the reader is referred to the web version of this article).

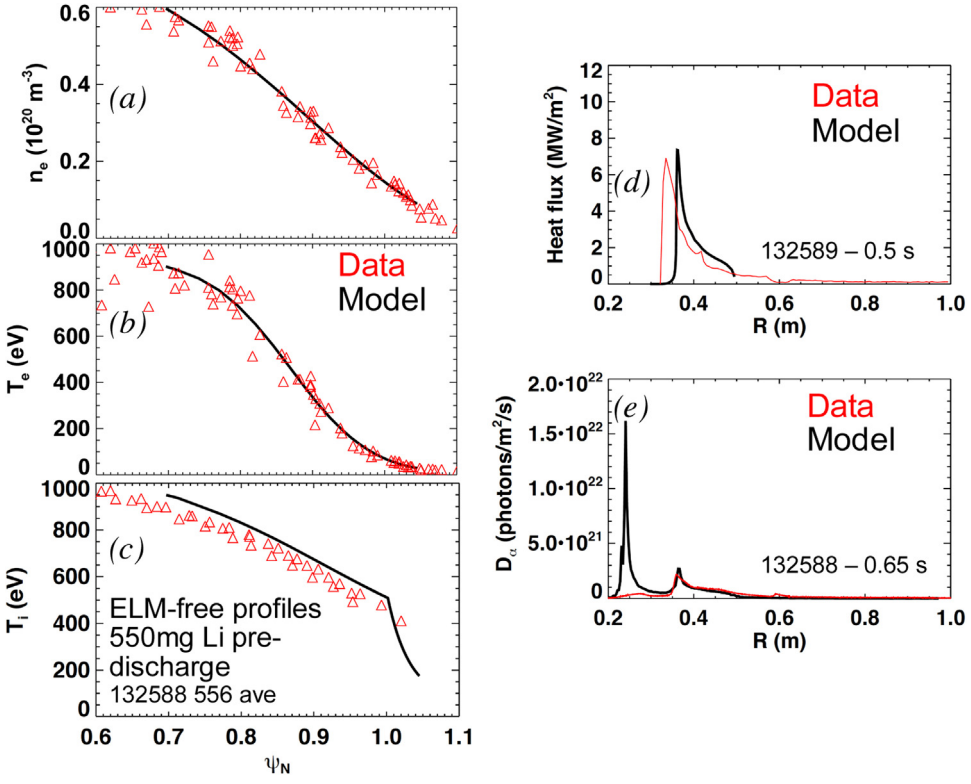

Fig. 7. Composite plasma profiles synced to the last 50% of the ELM cycle from reference boronized discharges with 6 MW NBI power: (a) electron density n_e, (b) electron temperature T_e, and (c) ion temperature T_i, The red symbols are data, and the solid black curve comes from SOLPS modeling. The lower divertor heat flux and peak Dα are shown in panels (d) and (e) respectively (for interpretation of the references to colour in this figure legend, the reader is referred to the web version of this article).

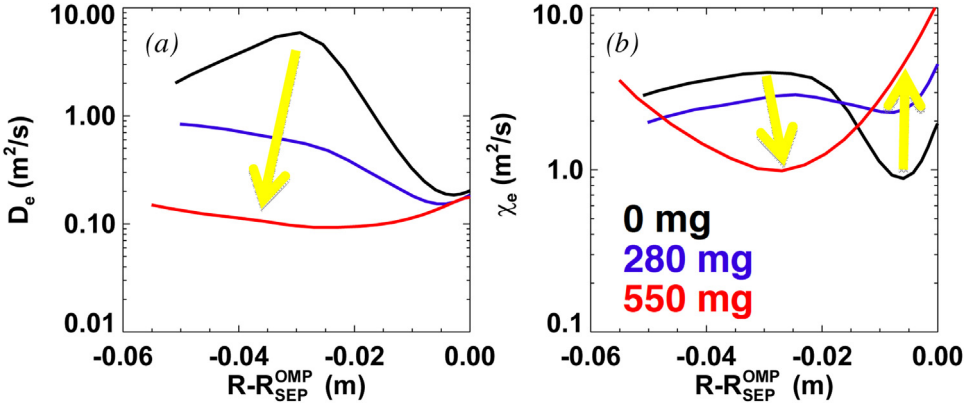

Fig. 8. (a) Effective electron particle diffusivity D_e and (b) electron thermal conductivity χ_e vs. distance from the separatrix at the outer midplane. The yellow arrows indicate increasing levels of pre-discharge dose.

stack radius in NSTX-U. In addition, the fact that these plasmas responded in a similar manner to the dose scan in the moderately shaped discharges where the centroid of lithium deposition was 50 cm away from the outer strike point suggests that the positive effects of lithium coatings had saturated. Additional reduction in recycling, and possible further improvements in confinement, may require liquid lithium PFCs or greater wall coverage of solid PFCs, as observed e.g. in LTX [13]; such a flowing liquid lithium divertor upgrade is planned for NSTX-U.

Acknowledgements

This research was sponsored in part by U.S. Dept. of Energy under contracts DE-AC02-09CH11466, DE-AC05-00OR22725, DE-FC02-04ER54698, DE-FC02-99ER54512 and DE-AC52-07NA27344. We greatfully acknowledge the contributions of the NSTX operations staff. The digital data for this paper can be found at: http://arks.princeton.edu/ark:/88435/dsp01h128nh17k.

References

[1] D.K. Mansfield, et al., Phys. Plasmas 3 (1996) 1892.
[2] G.L. Jackson, et al., J. Nucl. Mater. 241 (1997) 655.
[3] H.W. Kugel, et al., J. Nucl. Mater. 363–365 (2007) 791.
[4] D.K. Mansfield, et al., Nucl. Fusion 41 (2001) 1823.
[5] D.K. Mansfield, et al., Fusion Eng. Des. 85 (2010) 890.
[6] T.H. Osborne, et al., Nucl. Fusion 55 (2015) 063018.
[7] J.S. Hu, et al., Phys. Rev. Lett. 114 (2015) 055001.
[8] D.K. Mansfield, et al., Nucl. Fusion 53 (2013) 113023.
[9] A. Bortolon, et al., Nucl. Fusion 56 (2016) 056008.
[10] M.A. Jaworski, et al., Nucl. Fusion 53 (2013) 083032.
[11] M.L. Apicella, et al., Plasma Phys. Control Fusion 54 (2012) 035001.
[12] R. Majeski, et al., Bull. Am. Phys. Soc. 56 (2011) 245.
[13] J.C. Schmitt, et al., Phys. Plasmas 22 (2015) 056112.
[14] J. Ren, et al., Phys. Scr. T159 (2014) 014033.
[15] J.S. Hu, et al., Nucl. Fusion 56 (2016) 046011.
[16] F.L. Tabarés, Plasma Phys. Control Fusion 58 (2016) 014014.
[17] F.L. Tabarés, et al., Plasma Phys. Control Fusion 50 (2008) 124051.
[18] H.W. Kugel, et al., J. Nucl. Mater. 390–391 (2009) 1000.
[19] H.W. Kugel, et al., Phys. Plasmas 15 (2008) 056118.
[20] H.W. Kugel, et al., J. Nucl. Mater. 363–365 (2007) 791.
[21] M.G. Bell, et al., Plasma Phys. Control Fusion 51 (2009) 124054.
[22] D.K. Mansfield, et al., J. Nucl. Mater. 390–391 (2009) 764.
[23] R. Maingi, et al., Phys. Rev. Lett. 103 (2009) 075001.
[24] D.P. Boyle, et al., Plasma Phys. Control Fusion 53 (2011) 105011.
[25] R. Maingi, et al., Nucl. Fusion 52 (2012) 083001.
[26] R. Maingi, et al., Phys. Rev. Lett. 107 (2011) 145004.
[27] J.M. Canik, et al., J. Nucl. Mater. 415 (2011) S409.
[28] D. Boyle, et al., J. Nucl. Mater. 438 (2013) S979.
[29] J.M. Canik, et al., Phys. Plasmas 18 (2011) 056118.
[30] R. Maingi, et al., J. Nucl. Mater. 463 (2015) 1134.
[31] V.A. Soukhanovskii, et al., Proc 23rd Fusion Energy Conference, Daejon Korea11-16 Oct 2010, 2010, pp. 3–32 (paper EXD-2010).
[32] S.M. Kaye, For the ITER confiement and transport database working group, Nucl. Fusion 37 (1997) 1303.
[33] F. Scotti, et al., Nucl. Fusion 53 (2013) 083001.
[34] R. Schneider, Contrib. Plasma Phys. 46 (2006) 3.
[35] V.A. Soukhanovskii, et al., Rev. Sci. Instrum. 74 (2003) 2094.
[36] C.S. Pitcher, P.C. Stangeby, Plasma Phys. Control Fusion 39 (1997) 779.
[37] J.M. Canik, et al., Nucl. Fusion 53 (2013) 113016.
[38] J.E. Menard, et al., Nucl. Fusion 52 (2012) 083015.